Topology optimized multi-material self-healing actuator with reduced out of plane deformation

Wang, Zhanwei; Terryn, Seppe; Legrand, Julie; Ferrentino, Pasquale; Kashef Tabrizian, Seyedreza; Brancart, Joost; Roels, Ellen; Van Assche, Guy; Vanderborght, Bram

Published in:
2022 IEEE/RSJ International Conference on Intelligent Robots and Systems

DOI:
10.1109/IROS47612.2022.9981297

Publication date:
2022

Document Version:
Accepted author manuscript

Topology optimized multi-material self-healing actuator with reduced out of plane deformation

Zhanwei Wang[1*], Seppe Terryn[1], Julie Legrand[1], Pasquale Ferrentino[1], Seyedreza Kashef Tabrizian[1], Joost Brancart[2], Ellen Roels[1], Guy Van Assche[2] and Bram Vanderborght[1]

1) Brubotics, Vrije Universiteit Brussel and Imec, Pleinlaan 2, 1050 Elsene, Belgium.

2) Physical Chemistry and Polymer Science, Vrije Universiteit Brussel, Pleinlaan 2, 1050 Elsene, Belgium.

***Abstract*—Recent advances in soft robotics in academia have led to the adoption of soft grippers in industrial settings. Due to their soft bending actuators, these grippers can handle delicate objects with great care. However, due to their flexibility, the actuators are prone to out-of-plane deformations upon asymmetric loading. These undesired deformations lead to reduced grasp performance and may cause instability or failure of the grip. While the state-of-the-art contributions describe complex designs to limit those deformations, this work focuses on a complementary path investigating the material distribution. In this paper, a novel bending actuator is developed with improved out-of-plane deformation resistance by optimizing the material distribution in multi-material designs composed of two polymers with different mechanical properties. This is made possible by the strong interfacial strength of Diels-Alder chemical bonds in the used polymers, which have a self-healing capability. A Solid Isotropic Material with Penalization (SIMP) topology optimization is performed to increase the out-of-plane resistance. The actuator is simulated using FEA COMSOL in which the (hyper) elastic materials are simulated by Mooney-Rivlin models, fitted on experimental uniaxial tensile test data. This multi-material actuator and a reference single material actuator were manufactured and modeled. Via experimental characterization and validation in FEA simulations, it is shown that the actuator performance, characterized by the in-plane performance and out-plane resistance, can be increased by an optimized multi-material composition, without changing the geometrical shape of the actuator.**

***Index Terms*—Soft robotics; Topology Optimization; Multi-material; Finite element method; Self-healing polymers**

I. Introduction

Inspired by biological tissue, synthetic hyperelastic polymers can introduce compliance and versatility in soft robotics. The soft bodies of this new generation of robots are made from hyperelastic materials (e.g. silicons or polyurethanes), resulting in continuously deformable structures with complex actuation modes [1]. Soft grippers, an important field in soft robotics, are highly adaptable when in contact with an object, making them ideal candidates to grasp delicate parts, including food, electronics and even corals. Recently soft grippers have shown their potential, as achievements in academia have led to industrial adoption of grippers in the agrifood industry. Compared to conventional rigid grippers, soft robots are safe, being highly flexible and compliant. Consequently, soft grippers can be used for safe human-robot interactions in applications like prosthetics, exoskeletons, collaborative robots, social robots and minimal invasive surgery.

However, being hyperelastic, the actuators in a gripper are challenging to control [2] and can undergo undesired deformations when in contact with an object. More specifically, out-of-plane deformations of bending actuators in grippers, caused by, e.g., gravity, inclined surfaces or design inaccuracies can lead to imprecise soft system control as well as poor grasping performance. In order to tackle the problem, Jiang et al. stiffen the bending actuators in the gripper by granular jamming, enhanced out-of-plane resistance [3]. Although this approach is successful, the use of vacuum driven granular jamming highly increases the complexity of the system and consequently its control.

Scharff et al. developed a stiffening structure for improving the out-of-plane stiffness [4]. Actuators with higher out-of-plane stiffness can exert higher in-plane force, which was taken as a performance index. The optimized actuator structure could exert 70% higher in-plane force compared to the reference actuator with no stiffening structure. Tawk et al. used a meta-material approach to reduce out-of-plane deformation [5]. By increasing the contact surface and reduced contact force, their grasp is more stable. These geometrical optimizations also have their limitations, as the stiffening structures make the actuators more bulky, can interfere with the grasping object and are not easily miniaturized.

In this paper, we propose to tackle the out-of-plane deformations by topology optimization of a multi-material actuator for a soft gripper. Multi-material soft structures have been of increasing interest due to their potential to build more complex and versatile actuators [6]. Other than manual designs derived from engineering experience and biological inspiration, there have been efforts to optimize soft robots based on heuristic algorithms. Voxel-based multi-material robot simulators are developed for evolutionary optimization, which contributes significantly on locomotion simulations of robots by improving computation efficiency [7]–[9]. The isotropic volumetric expansion and contraction is difficult to realize in reality and consequently physical voxel fabrication is rare and the resulting soft robots have limited performance [10]–[12]. Topology optimization methods have been applied for reducing manufacturing cost and realizing desired mechanical behaviors. A cable-driven gripper was designed through level set-based topology [13], and a pneumatic gripper was designed by solid isotropic material with penalization method (SIMP) [14]. Both

*Corresponding authors email: zhanwei.wang@vub.be

of them improved performance compared to reference grippers. Multi-material topology optimization is a fast developing sub field, but is mostly still limited to planar algorithm improvement [13], [15], [16]. Only few 3D algorithms have been developed and these are not compatible to optimize complex geometry. Chih-Hsing et al. developed a multi-material topology optimization method and tested it by optimizing a gripper output displacement and force. The multi-material behavior is created in a single part by varying the infill density during fused filament fabrication printing [17].

The objective of this work was to improve out-of-plane deformation resistance of a bending actuator without changing the geometrical shape of the actuator and without losing any in-plane bending performance. To do so, we focused solely on adapting the material composition of the actuator. Although the methodology described in this paper can be applied to various types of bending actuators, actuated by different principles including pneumatically and tendon driven. We selected a single pneumatic actuator design given in Fig. 1a. It is investigated if a material composition using two hyperelastic materials with different mechanical properties can result in a multi-material actuator with an in-plane bending performance that is identical to a single material actuator (Fig. 1b, blue), but with improved out-of-plane deformation resistance (Fig. 1b, green). The optimization is performed using a Finite Element Method (FEM) model in COMSOL in which the mechanical behavior of the elastomeric polymers is described by hyperelastic constitutive laws. An optimal distribution pattern of the two hyperelastic materials in actuator is obtained via the Solid Isotropic Material with Penalization (SIMP) method. The optimized design is manufactured to validate the simulations and is bench marked against a reference actuator, composed of a single hyperelastic material. This is done by analyzing the in-plane and out-of plane deformation of the actuators in a dedicated experimental setup [18]. Next, the validated simulation and the optimized material distribution are used to further study the influence of the ratio between the Young's modulus of the two materials on the out-of-plane deformation resistance.

Many multi-material soft robots fail after limited actuation cycles due to interfacial debonding. At the multi-material interfaces, stress concentration lead to the debonding of the interface, as adhesion relies on weak interfaces and eventually failure [19]. For pneumatically driven actuators this leads to bursts or tears, resulting in a drop in efficiency and eventually in complete failure. The strength of these multi-material interfaces can be largely increased when building the actuator out of reversible covalent elastomers, e.g., Diels-Alder polymers. As illustrated by the authors in previous papers [6], [20], robust multi-material actuators were made by joining two flexible parts, manufactured out of two Diels-Alder polymers with different mechanical properties, using a heat-cool cycle (90°C). Upon heating and cooling, strong covalent bonds are formed at the interface. Because of these advantages Diels-Alder polymers were selected for developing the optimized multi-material bending actuator. In addition, these polymers have a healing capacity, as large cuts and tears can be healed by exposing the materials or the actuator to an elevated temperature (90°C), as will be illustrated in this paper.

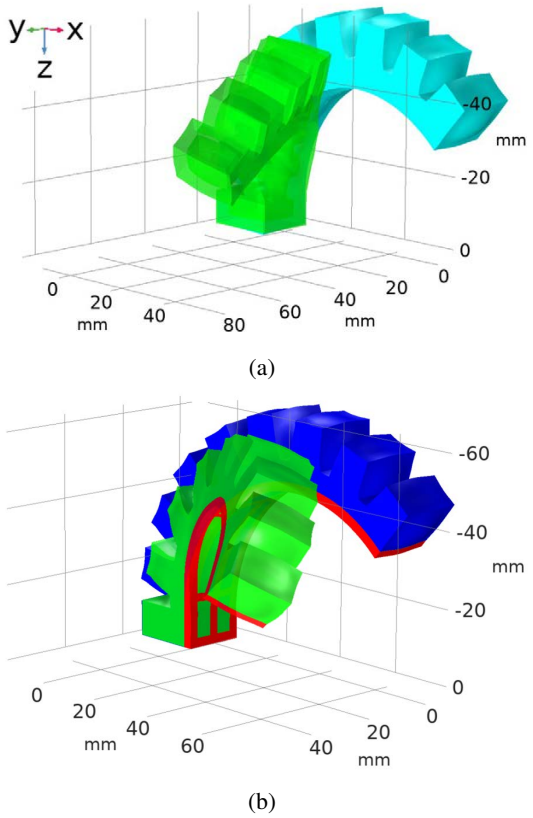

Fig. 1: The simulated actuator deformation includes out-of-plane bending (green) and in-plane bending (blue). The upper figure is single material reference actuator composed of DPBM-FT5000-r0.58 (light blue), the bottom figure is multi-material optimized actuator, composed of DPBM-FT5000-r0.5 (dark blue) and DPBM-FT3000-r1 (red).

II. Modeling and Optimization

A. Fitting constitutive material models

Although the actuator can be optimized using a large number of hyperelastic materials, each having different mechanical properties, this paper focuses on the optimization using two materials. We selected two reversible Diels-Alder polymer networks, DPBM-FT3000-r1 and DPBM-FT5000-r0.5 to be used in the multi-material actuator design. Aside from being self-healing due to their reversible crosslinks [21], these materials have different mechanical properties as illustrated by tensile testing shown in Fig. 2. These were obtained by straining $30\times5\times1\,\text{mm}^3$ samples with a rate of $1\%\text{s}^{-1}$. This is emphasized by the difference in the Young's modulus (Table I), calculated as the slope of a linear regression line in the 0-5% strain window. Nevertheless, these reversible polymers allow creating strong interfacial covalent bonding at the interface of the two materials [6], [20]. Consequently, the multi-material interfaces are robust, in contrast to the weak multi-interfacial bonding found in soft robots build out of traditional materials like silicone or polyurethane. This is an important characteristic for soft pneumatic actuators as weak multi-material interfaces

can delaminate as a result of stress concentrations during actuation, leading to air leaks and eventually complete failure of the actuator. These two hyperelastic materials are modeled in a FEM simulation using the Moonley-Rivlin constitutive material law. The Moonley-Rivlin model, composed of five parameters, was fitted onto experimental stress-strain data derived via tensile testing of both materials (Table I). This fitting was performed in Abaqus using the Levenberg-Marquardt method [18] and can be seen in Fig. 2.

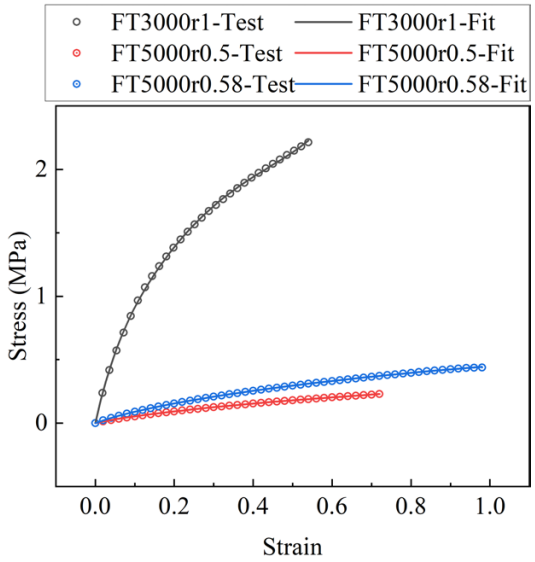

Fig. 2: The uni-axial tensile stress-strain data for DPBM-FT5000-r0.5, DPBM-FT3000-r1, DPBM-FT5000-r0.58 and corresponding Mooney-Rivlin hyperelastic material model fitting curves.

TABLE I: The hyperelastic model parameters of the self-healing materials (Unit: MPa)

Parameters	**Materials**		
	FT5000-r0.5	***FT3000-r1***	***FT5000-r0.58***
Young's modulus	0.64	22.16	1.09
D1[a]	1.10	0.053	0.67
C10	-0.15	1.10	-0.10
C01	0.26	0.52	0.29
D2[a]	0	0	0
C20	0.18	-8.91	0.035
C11	-0.61	26.9	-0.15
C02	0.59	-21.1	0.23

[a] The unit of D1 and D2: MPa^{-1}.

B. Topology optimization

For this work a bending soft pneumatic actuator (BSPA) was selected, based on the PneuNet design, a classic and extensively used actuator in both academia and industrial applications. The geometrical dimensions of this actuator can be found in Fig. 3, and are similar to the design in a previous publication [18]. The geometric structure parameters are fixed, and out-of-plane deformation is addressed solely by changing the material distribution in the actuator. To optimize the material's spatial distribution in a fixed actuator geometry and to simplify the computational complexity, several manual designs were simulated in COMSOL using the hyperelastic material laws of the two materials, to roughly evaluate the influence of varying the stiffness in different parts of the actuator Fig. 2. From this first analysis, it could be concluded that material distribution modification on the bottom part of the actuator affects less the in-plane bending, while reducing out-of-plane deformation under lateral force loads. This is because the material located on the bottom part stretches less during actuation and mainly bends. Therefore topology optimization is employed on the bottom part to get an optimal stiff material distribution with a lower volume ratio to reduce the influence on the bending angle. In addition, a high-volume ratio of soft material is desired at the contact surface to enhance adaptability and safety in soft grippers.

The Solid Isotropic Material with Penalization (SIMP) topology optimization method is adopted to perform actuator optimization. Its density model involves the definition of a control variable field, θ_c, which is bounded between 0 and 1. In solid mechanics, θ_c=1 corresponds to the material from which the stiff material is to be built, while θ_c=0 corresponds to a very soft material. The hyperbolic tangent function is applied in a Helmholtz filter to avoid the grayscale, which shows clearer physical interpretation. The SIMP approach with penalty factor incorporated is given as:

$$E_p = E\theta_p; \theta_p = \theta_{\min}(1-\theta_{\min})\theta^{p_{\text{SIMP}}}$$

Where E: Young's modulus for the solid material, E_p: The penalized Young's modulus, p: Penalization parameter for intermediate density, θ_p: Penalized material volume, $\theta_{\min}$: Minimum Penalized material volume, θ: Material volume factor.

The optimization of the actuator bottom is simplified to a 2D case. The material distribution of a single sided clamped beam has to be optimized to minimize deformation while being exposed to a force on the non-clamped side. When implementing this optimized beam at the bottom of a 3D actuator, it will reduce the out-of-plane deformation. Because of symmetry and because out-of-plane deformation is bidirectional, only half of the beam has to be modeled, represented by a 8.25×101.5 mm^2 beam. This geometry and its boundary conditions are shown in Fig. 3a. The left end is fixed, while on the right end, a 1 N force is placed (on the blue line segment).

The goal of the SIMP topology optimization is to minimize the displacement of the tip in the x-direction (representing the out-of-plane deformation when embedded in the actuator). This minimal displacement is the object function, while the material distribution is the control variable. For every volume element two materials, DPBM-FT5000-r0.5 or DPBM-FT3000-r1, can be selected. As the use of the stiffer material DPBM-FT3000-r1, will impact the in-plane bending angle, the percentage volume share of the stiff material is constrained to not higher than 0.5. A stationary solver was used in the optimization. To make sure this optimization is mesh size independent, different mesh sizes (number of elements from 29010 up to 189039) were applied in the simulation, however, this did not change the outcomes of the simulation significantly. The final mesh used for the simulation contains 29010 elements.

The optimized material distribution is illustrated in Fig. 3a, in which the black zone represents the stiffer DPBM-FT3000-r1 and the white material is the flexible DPBM-FT5000-r0.5. This result was mirrored to create the bottom layer of the bending actuator, which was designed in Solidworks, according to the presented dimensions (Fig. 3b-d).

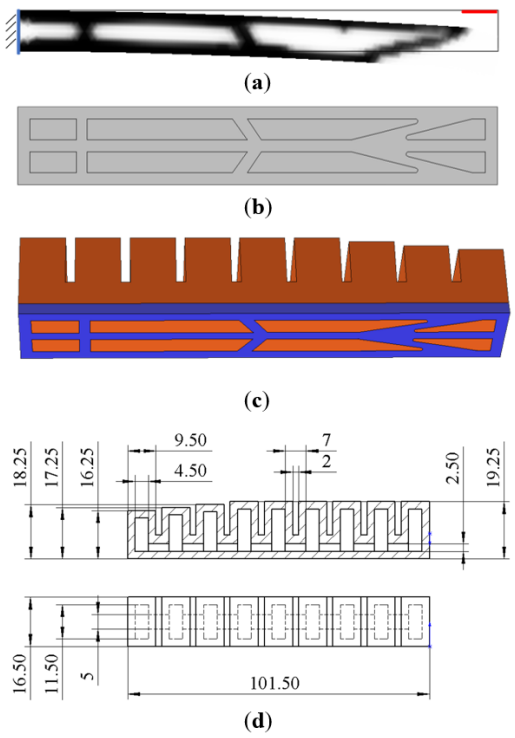

Fig. 3: **a**) Results of the topology optimization on the bottom of the actuator. The bottom of the actuator is simplified as a beam, representing half of the bottom of the actuator. (**b**) The bottom of the actuator is constructed by symmetry of reinforcing structure. (**c**) The 3D design of the multi-material actuator. (**d**) The design and dimensions of self-healing soft pneumatic actuator.

C. Modeling the out-of-plane resistance

To illustrate that higher out-of-plane resistance can be achieved using this optimized multi-material bending actuator, a reference single material bending actuator was selected. This reference bending actuator was made from a DPBM-FT5000-r0.58 Diels-Alder material. A slightly stiffer DPBM-FT5000-r0.58, compared to the r0.5 material, was selected such that the multi-material actuator and the reference single-material actuator have similar in plane performance. Also for this r0.58 material a Neo-Hookean constitutive material law was fitted onto uniaxial tensile testing data (Fig. 2 and Table I)

The actuator CAD design (Fig. 3d) is imported in COMSOL, in which the materials are modeled using the hyperelastic constitutive laws. The COMSOL FEA allows modeling the deformation upon pressurizing the inner chambers of the actuator (Fig. 1b, blue). The reference single material actuator composed of DPBM-FT5000-r0.58 is simulated. The base of the actuator is fixed, using a fixed boundary condition. For the in-plane deformation modeling, the gravitational force field is along the z-axis, while the pressure is increased incrementally until 138 kPa. The out-of-plane resistance is evaluated by placing a lateral force (1 N) at the actuator tip in the y-direction and by looking at the displacement in the y-direction (Fig. 1b, green). In this case the gravitational force field is along the y-axis. The y-displacement of the actuator tip is the metric for the out-of plane deformation, while the in-plane deformation is characterized by the bending angle between vertical line and segment between the actuator base and the actuator tip: $\beta = \arctan\left(\frac{\Delta X}{l-\Delta Z}\right)$, in which l is the length of the actuator.

The in-plane deformation and out-of-plane deformation contours in Fig. 1 have visually shown the out-of-plane force affected bending behavior. The relation between actuation pressure and the bending angle and out-of-plane deformation for the reference actuator fabricated by DPBM-FT5000-r0.58 are shown in Fig. 4. The bending angle increases linearly with increasing pressure, however, at higher pressures the bending angle growth rate increases slightly. This is caused by the non-linear hyperelastic constitutive material laws that were used in this FEA model (Fig. 2). At high strain, small increases in pressure, and therefore stress, create larger strain increments. The bending angle-pressure curves also show that the out-of-plane force can cause in-plane bending besides the intuitive out-of-plane bending. This bending angle will be invalid for grasping tasks. As pressurizing, the actuator with out-of-plane force has a lower bending angle compared to no out-of-plane load condition. This illustrates the loss of grasping performance upon out-of-plane deformation.

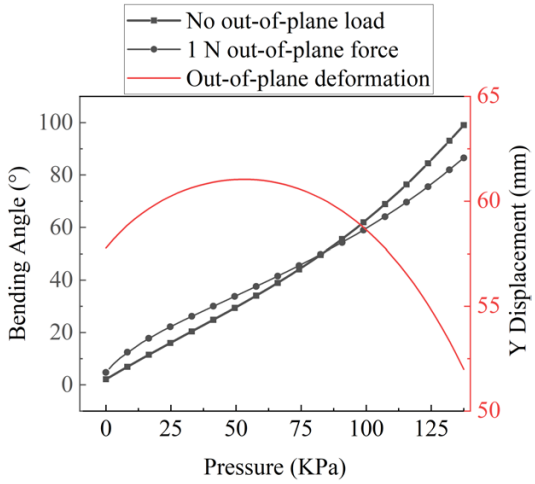

Fig. 4: Simulations on lateral force influence. The black curves show the relation between pressure and in-bending angle, the red curve shows the relation between pressure and out-of-plane deformation.

As seen in the Fig. 4, the out-of-plane deformation, represented by the y-displacement, increased upon increasing the pressure at low pressures. The out-of-plane deformation attains maximum around 60 kPa, then it shows a significant decreasing rate at higher pressure. To analyze this behavior, the wall bears an out-of-plane force W_u and the other side wall W_d are selected as objects, their average strain on surfaces are

expressed as S_t and S_s separately. They are shown in Fig. 5 with integral strain difference S. At the start, the pressure is 0 KPa, only out-of-plane force on the W_u, leading to out-of-plane bending. So S_t is higher than S_s, which means the upper surface W_u is more stretched. The strain difference among whole actuator derives 1.2 N total reaction confronts the external load. As pressurization, the whole actuator is inflated, S_s is faster increasing because W_d is initially less stretched compared to W_u, without enough stress to resist air-driven volume tension. This finally resulted in out-of-plane deformation stop increasing after 60 kPa, shown by the red curve in Fig. 4. The integral strain difference also attains maximum value, then it decreases as pressurization, which indicates the continually increasing air-pressure driven deformation gradually dominates compared to out-of-plane force driven deformation.

Besides, small disturbance at the start of the grasping behavior will change the actuator bending direction easily, usually causing instability and even failure to grasp [4]. Thus, the initial static out-of-plane stiffness, inner stress and strain distribution difference are key for reinforcing actuators to maintain the desired bending trajectory. Adapting highly hyperelastic materials will benefit to enhance the out-of-plane stiffness. The higher stress at small strain range benefits the stiffness, the lower stress increasing rate during larger strain range reduces needed actuation pressure.

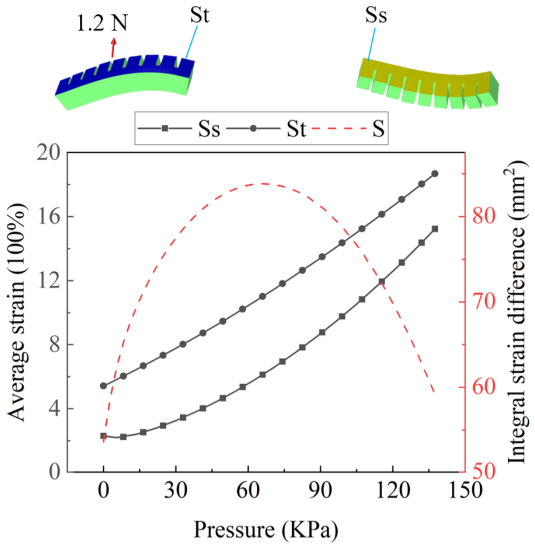

Fig. 5: The actuator side walls stress and strain analysis. W_t and W_s are integral stress on the wall bears out-of-plane force and the other side wall separately, integral stress difference and integral strain difference on two walls are shown by dotted curve and red curve separately.

III. Experimental Validation

A. Manufacturing of the actuator

The multi-material and reference single material actuators were fabricated to verify the simulations, the actuators are shown in Fig. 7e. The pneumatic chamber and bottom parts are manufactured separately. The top part, the pneumatic chambers are compression molded. Pellets of DPBM-FT5000-r0.5 or 0.58 are placed inside of a nylon mold (Fig. 7a) and heated to 120°C, above the material gel transition temperature (T_{gel}=95°C for r0.5 and T_{gel}=102°C for r0.58). Above their T_{gel}, the material liquefies into a viscous liquid, taking the shape of the mold. Next the inner mold is pushed into the outer mold using a hydraulic press, after which the entire part is cooled down to 25°C and demolded (Fig. 7b).

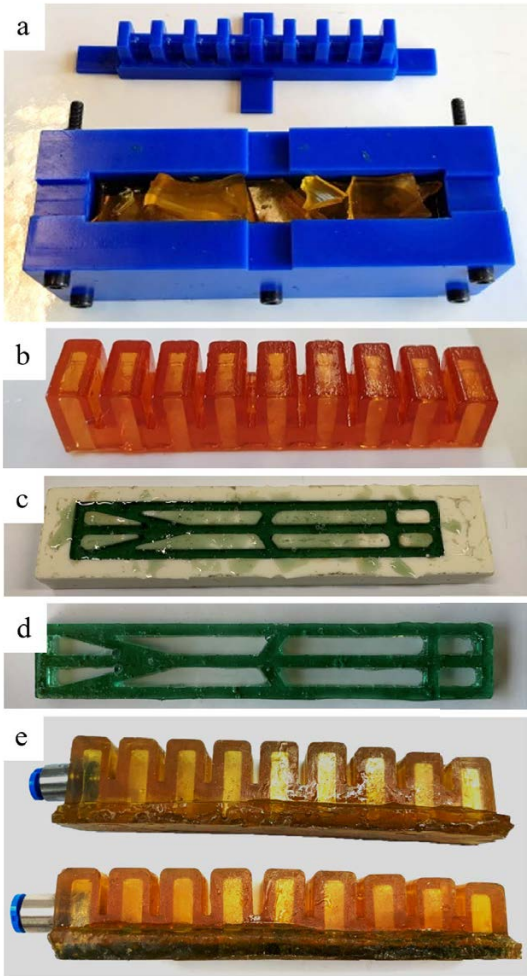

Fig. 6: Fabricated method for the bending pneumatic actuators. a) DPBM-FT5000-r0.5 or r0.58 pellets are placed in a nylon outer mold and heated to 120°C, above their gel transition temperature (T_{gel}). Consequently, the pellets degel into a viscous liquid, taking the shape of the mold. By compression molding the inner mold into the outer mold, the internal structure of the actuator is formed. b) Result of the compression molding step. c) The less flexible DPBM-FT3000-r1 material is cast in an epoxy mould by heating the material to 150°C, on which it degels into a liquid above its T_{gel}. d) Result of the casting step. e) The bottom and top part of the actuators are joined by chemically binding the parts together using strong covalent Diels-Alder bonds that result from a heat-cool cycle with an isothermal at 80°C for 1 hour.

In the manufacturing process of the bottom layer of the multi-material actuator, the stiff material structure is fabricated by casting as shown in Fig. 7c. To do so, DPBM-FT3000-r1 pellets

are placed on a nylon mold. By increasing the temperature to 150°C, above the materials degelation temperature (T_{gel} = 128°C), the material liquefies and flows into the shape (Fig. 7d). Next the soft material is cast in the hollow zones. This is done, by placing DPBM-FT5000-r0.5 pellets on top of the DPBM-FT3000-r1 structure. Upon heating to 120°C, the stiff material remains solid, while the soft material liquefies as its T_{gel} equals 95°C, flowing in between the stiff parts. Upon cooling, the flexible material solidifies and strong interfacial bonds are created between the two parts. For the single material actuator, the bottom part is made by placing pellets into a rectangular mold and heating the material to 120°C. Benefiting from materials intrinsic self-healing property, the top and bottom parts can be healed together by putting into an oven at 80°C for 1 hour and cooling down to 25°C. Upon this cooling process, strong covalent bonds are formed between the top and the bottom part, keeping the pneumatic actuator leak-tight.

B. Healing

The reversible cross-links in the Diels-Alder polymers, incorporate a healing capacity in both the single- and multi-material actuators. To illustrate this, the DPBM-FT5000-r0.58 actuator was cut in half using a scalpel blade. After bringing the fracture surfaces back in contact manually, the actuator was heated for 1 hour at 80°C. Upon cooling the Diels-Alder cross-links re-bond in the network, including across the fracture surface. The result is a full recovery of the actuator performance; the actuator is as good as new.

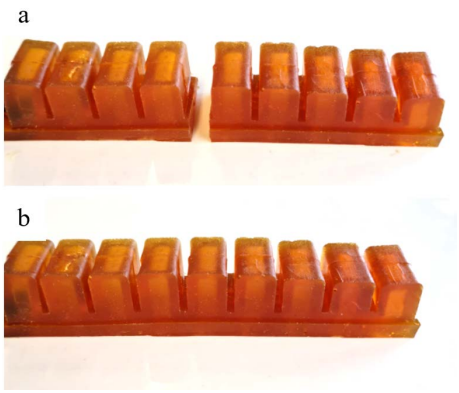

Fig. 7: Self-healing capacity of the DPBM-FT5000-r0.58 actuator. a) The actuator is cut in half. b) Via a heat treatment of 1 hour at 80°C the great damage can be completely healed.

C. Validation of the simulation

The manufactured actuators, both the multi-material and single-material prototype, were characterized in a dedicated test setup composed of a pressure regulator (FESTO, VEAB-L-26-D7-Q4-V1-1R1) that is connected to a compressed air source and a camera for deformation tracking (RGBD-camera). To control the regulator valve, an Arduino is used with a PWM signal and a low-pass filter. This is used to track the in-plane bending deformation as a function of internal pressure in the actuator (Fig. 8a), as well as out-of-plane deformation, resulting from placing a weight of 51 grams (=0.5 N) (Fig. 8c). To truly investigate the out-of-plane deformation, the actuator is actuated while this weight is hanging on the tip of the actuator (Fig. 8e). In addition, the multi-material and single-material actuator were compared based on FEA simulations in COMSOL using Mooney-Rivlin material laws for the simulation. To do so, also for DPBM-FT5000-r0.58, a hyperelastic Mooney-Rivlin law was fitted onto experimental tensile testing results using Abaqus (Fig. 2 and Table I). The simulations were used to evaluate the deformations for in-plane bending (Fig. 8b), as well as out-of-plane deformation (Fig. 8d), and this internal pressures varying from 0 - 55 kPa. Looking at the results of these

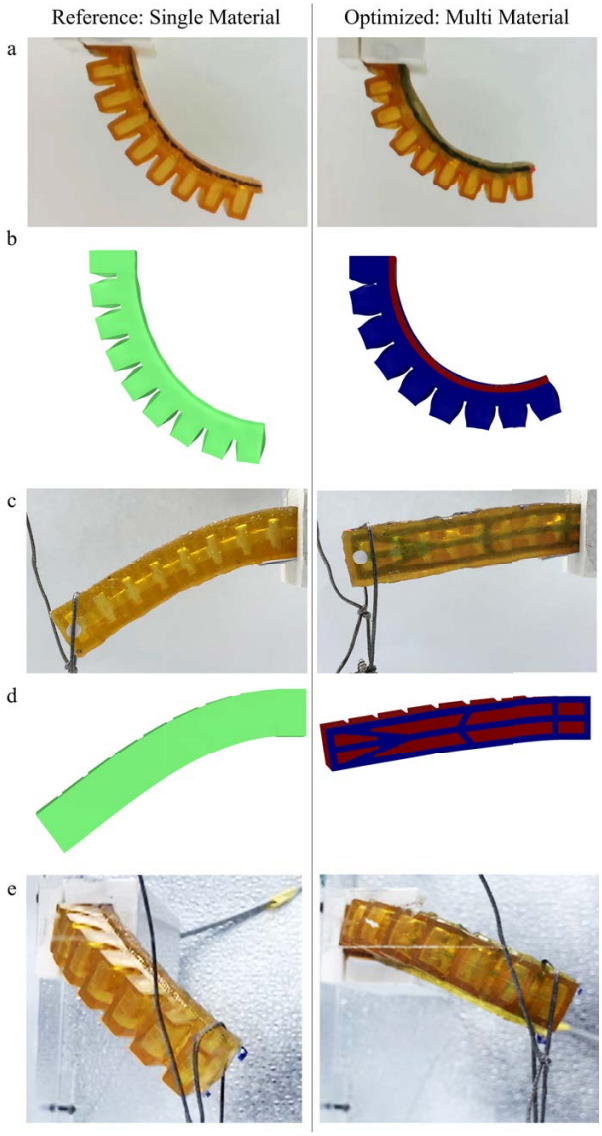

Fig. 8: Pictures of the experimental characterization in a dedicated test bench and images of the FEA modeling in COMSOL. a, b) The in-plane deformation at 55 kPa. c, d) The out-of plane displacement for non-pressurized actuators with a 0.5 N weight connected to the tip. e) The characterization of the out-of plane deformation during actuation/pressurization (55 kPa) while having a 0.5 N weight connected to the tip.

experiments and simulations (Fig. 9), we can firstly see that

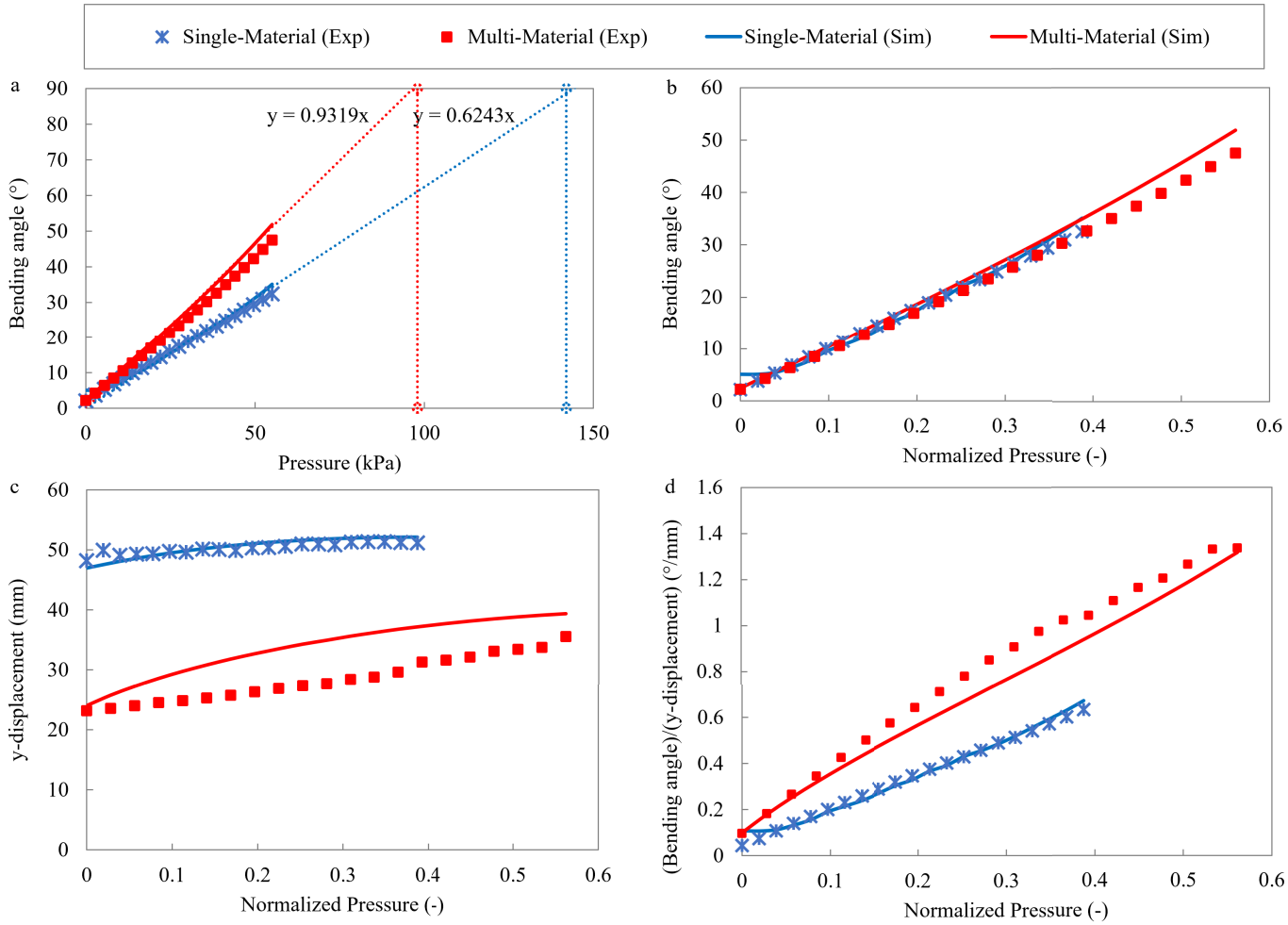

Fig. 9: Comparison of the single- and multi-material actuator via validation of the simulation using experimental characterization. a) The in-plane bending angle as a function of the internal pressure of the actuators. The relation is well approximated by a linear relationship which can be extrapolated to find the pressure at 90° bending angle. Using the pressure at 90°, the pressure can be normalized. b) Relation between bending angle and normalized pressure. As both the single material and multi-material actuator characteristic are linear and pressure is normalized, the cures overlay. c) The out-of plane deformation, characterized by the y-displacement, as a function of the normalized pressure. The multi-material actuator clearly has a higher out-of plane deformation resistance. d) The ratio between the bending angle and the y-displacement, as a function of pressure, is another metric to show the actuators bending vs out-of-plane resistance performance. It is clear that the multi-material actuator outperforms the single-material actuator.

the multi-material actuator has a higher in-plane performance, as it can reach higher bending angles as a function of pressure (Fig. 9a). This can result from the stiffer DPBM-FT3000-r1 bottom layer, which is known to assist the bending in PneuNet actuators [22]. It is also clear that the relationship between the bending angle and internal pressure can be linearly approximated. The simulations coincide well with the tests for the in-plane characterization for both actuators (Fig. 9a). This illustrates that the use of hyperelastic material models in COMSOL allow precisely modeling these pneumatic actuators, for small as well as large bending angles.

D. Comparison of the multi- and single-material actuator

To be able to compare these two actuators, the single- and multi-material one, the characterization curves in Fig. 9 were normalized. To do so, a linear relationship between bending angle and pressure was expressed for both actuators. Based on this and an extrapolation, the pressure at 90° bending angle is selected. The evaluated maximum pressure values shown in Fig. 9a are used to normalize the characterization data (Fig. 9 b, c and d). Consequently a bending angle of 90° corresponds to a normalized pressure of 1 for both actuators. As both actuators show a linear relationship between bending angle and time, the characterization curves are nearly identical (Fig. 9b).

This normalization allows comparing a single-material and multi-material actuator that have the same in-plane characteris-

tic (Fig. 9b), but completely different out-of plane resistance (Fig. 9c). It is clear that the optimized bottom layer in the multi-material actuator highly increases the out-of plane resistance, represented by the y-displacement, and this for all pressures. Consequently, this multi-material actuator is much more stable, while having the same in-plane bending characteristic. For the multi-material actuator, there is a slight difference between the simulated and experimentally measured out-of plane deformation, however, the same trend is clearly visible (Fig. 9c). These differences can be the results of fabrication or measurement errors; e.g., in the experiment a 0.5 N weight is attached to the end of the actuators, while in the simulation the force is applied directly on the side surface. In addition the actuator tends to twist, upon out-of-plane deformation leading to tracking challenges for the camera. To characterize the grasping effectiveness, the ratio of in-plane bending angle and out-of-plane displacement is calculated (Fig. 9d). The higher this ratio, the lesser the actuator is affected by out-of-plane disturbance. This performance ratio is twice as high for the multi-material actuator.

IV. Conclusions

This paper introduces a new approach to improve the out-of plane deformation resistance of bending pneumatic actuators by changing and optimizing the multi-material composition using two (hyper)elastic materials. The optimization was performed by a Solid Isotropic Material with Penalization (SIMP) topology optimization method in COMSOL. The actuator is composed of two Diels-Alder polymers which strongly bind together, creating a robust multi-material prototype. As a reference, a single material bending actuator was designed, manufactured and modeled as well. The actuators are simulated using FEA COMSOL in which the (hyper)elastic materials are simulated by (Neo-)Hookean laws, fitted on experimental uni-axial tensile testing data. Using a dedicated test bench, including a pressure controller and deformation tracking, both the in-plane characteristic as well as the out-of plane deformations are analyzed. Taking fabrication and measurement errors in account, the FEA simulators are validated and are a good representation for the experimental results. Using both simulations and prototyping, is proved that by optimizing the material distribution in bending pneumatic actuators, higher performance can be created; achieved by higher in-plane bending for fewer pressure, combined with a higher out-of-plane stiffness. As such this strategy can be used to create improved actuators for soft grippers with improved gripping performance, while having identical geometrical dimensions. Consequently, existing gripper systems do not have to be adapted in order to use these improved actuators.

ACKNOWLEDGMENT

This research is funded by the EU FET Project SHERO (828818). Zhanwei Wang is funded by China Scholarship Council (CSC). The FWO (Fonds Wetenschappelijk Onderzoek) funded the work through personal grants of Seppe Terryn (1100416N) and Ellen Roels (1S84120N). Seyedreza Kashef Tabrizian is funded by the EU Marie Curie ITN project SMART (860108).

References

[1] C. Lee, M. Kim, Y. J. Kim, N. Hong, S. Ryu, H. J. Kim, and S. Kim, "Soft robot review," *International Journal of Control, Automation and Systems*, vol. 15, no. 1, pp. 3–15, 2017.

[2] D. Rus and M. T. Tolley, "Design, fabrication and control of soft robots," *Nature*, vol. 521, no. 7553, pp. 467–475, 2015.

[3] Y. Jiang, D. Chen, C. Liu, and J. Li, "Chain-Like Granular Jamming: A Novel Stiffness-Programmable Mechanism for Soft Robotics," *Soft Robotics*, vol. 6, no. 1, pp. 118–132, 2019.

[4] R. B. Scharff, J. Wu, J. M. Geraedts, and C. C. Wang, "Reducing Out-of-Plane Deformation of Soft Robotic Actuators for Stable Grasping," in *2019 2nd IEEE International Conference on Soft Robotics (RoboSoft)*. IEEE, 2019, pp. 265–270.

[5] C. Tawk, R. Mutlu, and G. Alici, "A 3D Printed Modular Soft Gripper Integrated With Metamaterials for Conformal Grasping," *Frontiers in Robotics and AI*, vol. 8, p. 799230, 2022.

[6] E. Roels, S. Terryn, J. Brancart, G. Van Assche, and B. Vanderborght, "A Multi-Material Self-Healing Soft Gripper," in *2019 2nd IEEE International Conference on Soft Robotics (RoboSoft)*. IEEE, 2019, pp. 316–321.

[7] J. Hiller and H. Lipson, "Dynamic Simulation of Soft Multimaterial 3D-Printed Objects," *Soft Robotics*, vol. 1, no. 1, pp. 88–101, 2014.

[8] N. Cheney, J. C. Bongard, and H. Lipson, "Evolving Soft Robots in Tight Spaces," *Proceedings of the 2015 Annual Conference on Genetic and Evolutionary Computation*, p. 8, 2015.

[9] S. Kriegman, S. Walker, D. S. Shah, M. Levin, R. Kramer-Bottiglio, and J. Bongard, "Automated Shapeshifting for Function Recovery in Damaged Robots," in *Robotics: Science and Systems XV*. Robotics: Science and Systems Foundation, 2019.

[10] J. Hiller and H. Lipson, "Automatic Design and Manufacture of Soft Robots," *IEEE Transactions on Robotics*, vol. 28, no. 2, pp. 457–466, 2012.

[11] S. Kriegman, D. Blackiston, M. Levin, and J. Bongard, "A scalable pipeline for designing reconfigurable organisms," *Proceedings of the National Academy of Sciences*, vol. 117, no. 4, pp. 1853–1859, 2020.

[12] S. Kriegman, A. M. Nasab, D. Shah, H. Steele, G. Branin, M. Levin, J. Bongard, and R. Kramer-Bottiglio. Scalable sim-to-real transfer of soft robot designs.

[13] F. Chen, W. Xu, H. Zhang, Y. Wang, J. Cao, M. Y. Wang, H. Ren, J. Zhu, and Y. F. Zhang, "Topology Optimized Design, Fabrication, and Characterization of a Soft Cable-Driven Gripper," *IEEE Robotics and Automation Letters*, vol. 3, no. 3, pp. 2463–2470, 2018.

[14] H. Zhang, M. Y. Wang, F. Chen, Y. Wang, A. S. Kumar, and J. Y. H. Fuh, "Design and development of a soft gripper with topology optimization," in *2017 IEEE/RSJ International Conference on Intelligent Robots and Systems (IROS)*. IEEE, 2017, pp. 6239–6244.

[15] W. Zuo and K. Saitou, "Multi-material topology optimization using ordered SIMP interpolation," *Structural and Multidisciplinary Optimization*, vol. 55, no. 2, pp. 477–491, 2017.

[16] P. Liu and Z. Kang, "Integrated topology optimization of multi-component structures considering connecting interface behavior," *Computer Methods in Applied Mechanics and Engineering*, vol. 341, pp. 851–887, 2018.

[17] C.-H. Liu, Y. Chen, and S.-Y. Yang, "Topology Optimization and Prototype of a Multimaterial-Like Compliant Finger by Varying the Infill Density in 3D Printing," *Soft Robotics*, p. soro.2020.0212, 2021.

[18] P. Ferrentino, S. K. Tabrizian, J. Brancart, G. V. Assche, B. Vanderborght, and S. Terryn, "FEA based inverse kinematic control on hyperelastic material characterisation of self healing soft robots," *IEEE ROBOTICS AND AUTOMATION MAGAZINE.*, p. 9, 2021.

[19] S. Terryn, J. Langenbach, E. Roels, J. Brancart, C. Bakkali-Hassani, Q.-A. Poutrel, A. Georgopoulou, T. George Thuruthel, A. Safaei, P. Ferrentino, T. Sebastian, S. Norvez, F. Iida, A. W. Bosman, F. Tournilhac, F. Clemens, G. Van Assche, and B. Vanderborght, "A review on self-healing polymers for soft robotics," *Materials Today*, vol. 47, pp. 187–205, 2021.

[20] S. Terryn, E. Roels, J. Brancart, G. V. Assche, and B. Vanderborght, "Self-Healing and High Interfacial Strength in Multi-Material Soft Pneuumatic Robots via Reversible Diels-Alder Bonds," *Actuators*, vol. 9, p. 2: 34, 2020.

[21] S. Terryn, J. Brancart, D. Lefeber, G. Van Assche, and B. Vanderborght, "Self-healing soft pneumatic robots," *Science Robotics*, vol. 2, no. 9, p. eaan4268, 2017.

[22] D. Rus and M. T. Tolley, "Design, fabrication and control of soft robots," *Nature*, vol. 521, no. 7553, pp. 467–475, 2015.